HHS Public Access

Author manuscript

Nat Neurosci. Author manuscript; available in PMC 2017 May 21.

Published in final edited form as:

Nat Neurosci. 2017 January ; 20(1): 42–51. doi:10.1038/nn.4442.

A rapidly-acting glutamatergic ARC→PVH satiety circuit postsynaptically regulated by α-MSH

Henning Fenselau[1,*], **John N. Campbell**[1,*], **Anne M.J. Verstegen**[1,*], **Joseph C. Madara**[1], **Jie Xu**[1], **Bhavik P. Shah**[1], **Jon M. Resch**[1], **Zongfang Yang**[1], **Yael Mandelblat-Cerf**[1], **Yoav Livneh**[1], and **Bradford B. Lowell**[1,2,c]

[1]Division of Endocrinology, Diabetes and Metabolism, Department of Medicine, Beth Israel Deaconess Medical Center, Harvard Medical School, Boston, MA, USA, 02215

[2]Program in Neuroscience, Harvard Medical School, Boston, Massachusetts 02115, USA

Abstract

Arcuate nucleus (ARC) neurons sense the fed/fasted state and regulate hunger. Agouti-related protein (ARC^{AgRP}) neurons are stimulated by fasting, and once activated, they rapidly (within minutes) drive hunger. Pro-opiomelanocortin (ARC^{POMC}) neurons are viewed as the counterpoint to ARC^{AgRP} neurons. They are regulated in an opposite fashion and decrease hunger. However, unlike ARC^{AgRP} neurons, ARC^{POMC} neurons are extremely slow in affecting hunger (many hours). Thus, a temporally analogous, rapid ARC satiety pathway does not exist or is presently unidentified. Here, we show that glutamate-releasing ARC neurons expressing oxytocin receptor, unlike ARC^{POMC} neurons, rapidly cause satiety when chemo- or optogenetically manipulated. These glutamatergic ARC projections synaptically converge with GABAergic ARC^{AgRP} projections on melanocortin-4 receptor (MC4R)-expressing satiety neurons in the paraventricular hypothalamus (PVH^{MC4R} neurons). Importantly, transmission across the $ARC^{Glutamatergic}\rightarrow PVH^{MC4R}$ synapse is potentiated by the ARC^{POMC} neuron-derived MC4R agonist, α-MSH. This excitatory ARC→PVH satiety circuit, and its modulation by α-MSH, provides new insight into regulation of hunger/satiety.

[c]Corresponding author: Bradford B. Lowell, MD, PhD, blowell@bidmc.harvard.edu, Division of Endocrinology, Diabetes, and Metabolism, Department of Medicine, Beth Israel Deaconess Medical Center, Center for Life Sciences, Rm-703, 3 Blackfan Circle, Boston, MA 02115.

Correspondence and request for materials should be addressed to B.B.L. (blowell@bidmc.harvard.edu)

[*]These authors contributed equally to this work.

Author Contributions

H.F. and B.B.L. designed the experiments and analyzed data. J.N.C. performed the single cell RNA-seq experiments with help from Y.M.. H.F. and A.M.V. conducted the behavioral and histological studies with help from J.M.R. and Z.Y.. H.F. performed the electrophysiological experiments with help from J.C.M. and Y.L.. J.Y. generated *Pomc*-IRES-Cre mice. B.P.S. generated $Pomc^{lox}$ mice. H.F. and B.B.L. wrote the manuscript with comments from all of the authors.

The authors declare no competing financial interests.

Data availability

RNA-Seq data are available at Gene Expression Omnibus (GEO), accession number GSE81789. The authors declare that all other relevant data supporting the findings of this study are available on request.

Introduction

The ARC is located adjacent to the median eminence, which lacks a blood brain barrier. Unique properties that likely involve tanycytes allow circulating factors controlling energy balance such as leptin, insulin and various gut-secreted hormones to access ARC neurons[1, 2]. Importantly, the ARC contains two key opposing regulators of energy balance: ARC^{POMC} and ARC^{AgRP} neurons. ARC^{POMC} neurons release the MC4R agonist α-MSH and promote negative energy balance, whereas ARC^{AgRP} neurons release the MC4R antagonist AgRP, as well as the inhibitory transmitters GABA and NPY, to do the opposite. Evidence supporting this model is extremely robust. Ablation of ARC^{POMC} neurons[3, 4], or genetic deficiency of POMC[5, 6] or MC4R[7–10] results in hyperphagia and massive obesity. Ablation of ARC^{AgRP} neurons, on the other hand, causes starvation[11], while opto- or chemogenetic stimulation of ARC^{AgRP} neurons drives intense feeding[12, 13]. Indeed, the antagonistic "yin-yang" function of these two neurons is a constant feature of essentially all proposed models of homeostatic hunger/satiety regulation[14–16]. At odds with this widely held view, however, is the finding that opto- and chemo-genetic activation of ARC^{POMC} neurons fails to decrease feeding over a period of less than 8–12 hours of stimulation[4, 12, 17]. This is in striking contrast to the potent effect on hunger observed just minutes following ARC^{AgRP} neuron stimulation[12, 13, 18]. This lack of rapid effect strongly suggests that ARC^{POMC} neurons, by themselves, are not the full counterpoint to ARC^{AgRP} neurons. Based on this, we hypothesized that a functionally important, presently unknown neural component of the ARC-based homeostatic satiety system is missing from current models.

The paraventricular nucleus of the hypothalamus (PVH) is an important effector site for hunger/satiety regulation by ARC^{POMC} and ARC^{AgRP} neurons. ARC^{POMC} and ARC^{AgRP} neurons send dense projections to the PVH[19, 20], injection of MC4R ligands and NPY into the PVH potently affect feeding[20, 21], and, as determined via Cre/lox gene knockout studies, the hyperphagia-preventing actions of MC4Rs are mediated specifically by MC4Rs on PVH neurons[8, 22]. Importantly, ARC^{AgRP} neurons selectively, monosynaptically engage and consequently inhibit PVH^{MC4R} neurons[23] and optogenetic stimulation of ARC^{AgRP} terminals in the PVH stimulates intense feeding within minutes[23, 24]. Of note, the ability of ARC^{AgRP} terminal stimulation in the PVH to increase feeding is markedly blunted by concurrent light/ChR2 stimulation of the downstream PVH^{MC4R} neurons[23]. Thus, PVH^{MC4R} satiety neurons are important effectors of the ARC-based melanocortin system and as such exert marked control over hunger/satiety.

The ability of ARC^{AgRP} neurons to rapidly affect feeding relates to their release of the fast-acting inhibitory transmitters GABA and NPY[18, 24]. Blockade of either NPY1 receptors or $GABA_A$ receptors markedly attenuates the rapid feeding response to optogenetic ARC^{AgRP} terminal stimulation in the PVH[24]. Inhibition of melanocortin receptors via A^y-mediated ectopic expression of *agouti*, on the other hand, is without effect[12]. Similarly, in mice unable to release NPY or GABA from ARC^{AgRP} neurons, chemogenetic stimulation of ARC^{AgRP} neurons no longer affects feeding over a 2-hour period[18]. However, in these same mice, AgRP, working through MC4Rs, induces feeding but only after 4 hours of stimulation[18]. Thus, the ability of ARC^{AgRP} neurons to rapidly affect feeding depends upon release of the fasting-acting transmitters, GABA and NPY. AgRP (and subsequent MC4R inhibition)

effects feeding but only after a protracted period. Of interest, the reduced feeding seen following prolonged stimulation of ARC^{POMC} neurons is absent in A^{y} mice[12], suggesting that it is mediated by αMSH (and not GABA or glutamate). Consistent with the role of GABA in mediating rapid effects of AgRP neurons, light/ChR2-evoked release of transmitter from ARC^{AgRP}→PVH projections generates robust GABAergic IPSCs in PVH neurons[23–25]. In striking contrast, similar light/ChR2-evoked release studies in ARC^{POMC}→PVH projections are largely ineffective in generating either IPSCs or EPSCs in PVH neurons[26]. In total, the above findings are consistent with αMSH, as opposed to GABA and glutamate, being the relevant effector released by ARC^{POMC} neurons.

Given that rapid effects of ARC^{AgRP} neurons are mediated by release of fast-acting transmitters and that AgRP (MC4R antagonist) mediates only slow effects, and that PVH-projecting ARC^{POMC} neurons appear to release αMSH (MC4R agonist) but not fast-acting transmitters, we hypothesized that this transmitter profile of ARC^{POMC} neurons accounts for their slow and not fast suppression of feeding. Related to this, given that rapid effects of ARC^{AgRP} neurons are mediated by inhibitory transmitters, we hypothesized that a rapidly acting ARC satiety neuron, if it existed, would be excitatory and release the fast-acting transmitter, glutamate, onto PVH satiety neurons. Of interest, it was recently discovered that, by virtue of their expression of Nav1.7 (*Scn9a*), PVH neurons summate excitatory inputs over greatly extended timescales, allowing near-perfect integration of inputs magnifying their effects on neuronal firing[27]. Remarkably, genetic deletion of Nav1.7 in PVH neurons decreased their firing due to diminished summation of excitatory inputs and this resulted in massive obesity[27]. Thus, glutamatergic input from some presently unknown source plays a key role in regulating the activity of PVH satiety neurons, and subsequently hunger/satiety.

The majority of neurons in the ARC are GABAergic; far fewer are glutamatergic[28]. This raises the possibility that vesicular glutamate transporter 2 (ARC^{Vglut2}) neurons, or one of the few subsets of ARC^{Vglut2} neurons, has a specific function – for example, satiety. In the present study, we pursue the above-mentioned hypotheses and investigate the role of ARC^{Vglut2} neurons in regulating hunger/satiety.

Results

ARC^{Vglut2} neurons, unlike ARC^{POMC} neurons, rapidly promote satiety

To compare and contrast the temporal dynamics by which ARC^{POMC} neurons increase satiety, as well as another process they control - interscapular brown adipose tissue (iBAT) thermogenesis[16], Cre-dependent AAV-DIO-hM3Dq[13] was injected into the ARC of *Pomc*-Cre BAC transgenic mice[29] (Fig. 1a). Temperature transponders were implanted subcutaneously above iBAT to assess thermogenesis. Clozapine-N-oxide (CNO) effectively activated ARC^{POMC} neurons as evidenced by increased firing and induction of Fos (Supplementary Fig. 1a–d). As previously observed[4, 12], ARC^{POMC} neuron stimulation failed to rapidly decrease dark-cycle feeding (i.e., within 4 hours; Fig. 1b), but did decrease feeding after 24 and 48 hours (Supplementary Fig. 1e). In striking contrast, ARC^{POMC} neurons rapidly induced iBAT thermogenesis (Fig. 1c). This result demonstrates that ARC^{POMC} neurons, as a group, are capable of generating rapid responses. To ensure that failure to rapidly regulate satiety was not due to inadequate Cre expression by *Pomc*-Cre

BAC transgenic mice (e.g., in a specific subset of POMC neurons), we generated *Pomc*-IRES-Cre knockin mice (Supplementary Fig. 1f). Consistent with Cre being driven by the endogenous *Pomc* allele, Cre activity was restricted to the ARC, and within the ARC, to neurons immunopositive for POMC (Supplementary Fig. 1f–h). We next bilaterally transduced ARC^{POMC} neurons in *Pomc*-IRES-Cre mice with AAV-DIO-hM3Dq (Supplementary Fig. 1i). CNO administration effectively activated hM3Dq-expressing ARC^{POMC} neurons as assessed by induction of Fos (Supplementary Fig. 1j). Stimulation of ARC^{POMC} neurons in *Pomc*-IRES-Cre mice, however, again failed to rapidly suppress dark-cycle feeding (Fig. 1d). Thus, ARC^{POMC} neurons do not rapidly suppress feeding.

To determine if any ARC glutamatergic neurons rapidly induce satiety, we injected AAV-DIO-hM3Dq into the ARC of [Vglut2 (*Slc17a6*)-IRES-Cre] mice[28]. Vglut2 is the major glutamate synaptic vesicle transporter in the hypothalamus, hence Vglut2-IRES-Cre mice target relevant glutamatergic ARC neurons[28]. Small volumes (2–5 nl) were injected to avoid expression in neighboring, non-ARC areas (Supplementary Fig. 2a, b). hM3Dq/CNO stimulation of ARC^{Vglut2} neurons, in contrast to ARC^{POMC} neurons, rapidly and markedly suppressed feeding (Fig. 1e). To determine if ARC^{Vglut2} neurons are necessary, as well as sufficient for satiety, we transduced ARC^{Vglut2} neurons with AAV-DIO-hM4Di[13] (Supplementary Fig. 2a, c). CNO markedly inhibited hM4Di-expressing ARC^{Vglut2} neuron firing as evidenced by decreased firing (Supplementary Fig. 2d). Importantly, hM4Di/CNO-mediated inhibition of ARC^{Vglut2} neurons rapidly increased light-cycle feeding (Fig. 1f). Thus, ARC^{Vglut2} neurons rapidly and bidirectionally regulate satiety.

Fasting decreases ARC^{Vglut2} neuron activity

Given their role in promoting satiety, ARC^{Vglut2} neurons should be activated by feeding and inhibited by fasting. In agreement with this, we found that the firing rates of ARC^{Vglut2} neurons in brain slices from fasted mice, compared with fed mice, were considerably lower – indeed 13 of 17 neurons were silent (Fig. 2a). Consistent with reduced ARC^{Vglut2} neuron activity, fasting significantly increased both frequency and amplitude of spontaneous inhibitory postsynaptic currents (sIPSCs; Fig. 2b). The fasting-induced increase in sIPSCs raises the possibility that ARC^{Vglut2} neurons, like ARC^{POMC} neurons[24], are negatively regulated by GABAergic ARC^{AgRP} neurons. To probe connectivity between ARC^{AgRP} and ARC^{Vglut2} neurons, we performed ChR2-assisted circuit mapping (CRACM)[30, 31]. To this end, we stereotaxically injected AAV-DIO-ChR2-mCherry into the ARC of *Agrp*-IRES-Cre::Vglut2-IRES-Cre::*Npy*-hrGFP mice and recorded light-evoked inhibitory poststynaptic currents (IPSCs) in ARC^{Vglut2} neurons (mCherry-positive, GFP-negative; Fig. 2c). Light-evoked IPSCs, which were completely blocked by the $GABA_AR$ antagonist bicuculline, were detected in 13 of 14 $ARC^{AgRP} \rightarrow ARC^{Vglut2}$ neurons (Fig. 2c). Thus, ARC^{Vglut2} neurons, which are inhibited by fasting (Fig. 2a), receive strong GABAergic inhibitory input from hunger-inducing ARC^{AgRP} neurons, which are themselves activated by fasting[32].

$ARC^{Vglut2} \rightarrow$PVH projections, unlike $ARC^{POMC} \rightarrow$PVH projections, are effective in glutamatergic transmission

To determine if ARC^{Vglut2} neurons project to sites where ARC^{AgRP} and ARC^{POMC} neurons project and regulate hunger, we injected the anterograde tracer, AAV-DIO-Synaptophysin-

mCherry, into the ARC of Vglut2-IRES-Cre mice and performed immunohistochemistry for AgRP and POMC (Supplementary Fig. 3a–f). ARC^{Vglut2}, ARC^{AgRP} and ARC^{POMC} neurons projected to many of the same sites, including the PVH. Some ARC^{Vglut2} terminals in the PVH contained POMC but many did not (Supplementary Fig. 3d). Thus, ARC^{Vglut2} projections converge with hunger-regulating ARC^{AgRP} and ARC^{POMC} projections on downstream targets.

To compare ARC^{POMC}→PVH and ARC^{Vglut2}→PVH synaptic function, we performed CRACM on unidentified PVH (uPVH) neurons. We stereotaxically injected AAV-DIO-ChR2 into the ARC and recorded from unidentified PVH (uPVH) neurons in brain slices containing ChR2-expressing ARC terminals. When *Pomc*-Cre or *Pomc*-IRES-Cre mice were used, we failed to detect light-evoked excitatory postsynaptic currents (EPSCs) in any of 71 ARC^{POMC}→uPVH neurons tested (Fig. 3a, b). Given that ARC^{POMC} neurons express GABAergic markers (GAD isoforms)[33, 34], we also assessed if any PVH-projecting ARC^{POMC} neurons synaptically release GABA. Remarkably, we failed to detect light-evoked IPSCs in any of the 71 ARC^{POMC}→uPVH neurons tested (data not shown). In contrast, when Vglut2-IRES-Cre mice were used, we readily detected robust light-evoked EPSCs in many (12/30) ARC^{Vglut2}→uPVH neurons (Fig. 3c). The light-evoked EPSCs were mediated by glutamate as they were blocked by the α-amino-3-hydroxy-5-methyl-4-isoxazole propionic acid receptor (AMPAR) antagonist CNQX (Fig. 3c). Thus, ARC^{Vglut2} neurons, unlike ARC^{POMC} neurons, synaptically release glutamate onto PVH neurons. This raises the important possibility that the PVH is an important effector site of rapidly-acting ARC^{Vglut2} satiety neurons.

RNA-seq assessment of ARC^{Vglut2} satiety neurons

ARC^{Vglut2} neurons are a heterogeneous population that includes ARC^{POMC} neurons[33, 34] and fertility-regulating ARC^{Kiss1} neurons[35] though other subtypes may exist as well. To identify subtypes of ARC^{Vglut2} neurons, we profiled their gene expression using single-cell RNA-seq. Specifically, we isolated GFP-labeled neurons from the ARC of Vglut2-IRES-Cre::L10-GFP (loxSTOPlox-L10-GFP) mice (Fig. 4a) and sequenced their mRNA using the Smart-Seq2 RNA-seq method[36]. Since ARC neuron types are generally known for the neuropeptides they express, our first analysis focused on neuropeptide genes. A clustering analysis of 23 ARC^{Vglut2} neurons based on their expression of 90 neuropeptide genes showed three subpopulations (Supplemental Fig. 4a–c and Supplemental table 1). Specifically, we found that 44% were POMC neurons (the majority of which co-expressed cocaine- and amphetamine-regulated transcript peptide; *Cartpt*), 17% were *Kiss1*/*Tac2* neurons and 39% lacked a strong marker and so are annotated as “Other” neurons (Fig. 4b, c; Supplementary Fig. 4b). Consistent with the RNA-seq data, approximately 38% of ARC^{Vglut2} neurons are POMC neurons as assessed by immunohistochemistry (Fig. 4d; 105.4 ± 9.3 of 274.1 ± 10.3 GFP-positive cells were POMC-positive; mean ± SEM; counts from a total of 9 section, 3 sections from each of $n = 3$ mice; mice from multiple litters).

Given the absence of glutamatergic transmission from ARC^{POMC}→PVH neurons (Fig. 3a, b), we wondered if the *Pomc*-positive and *Pomc*-negative subtypes of ARC^{Vglut2} neurons differ in their expression of genes involved in synaptic transmission. We assigned ARC^{Vglut2}

neurons to *Pomc*-positive and *Pomc*-negative subsets based on their expression of *Pomc*, and then ranked genes according to the percentage of each ARC^{Vglut2} subset expressing the gene above a calculated expression threshold[37]. The analysis revealed that two genes encoding presynaptic molecules needed for fast, Ca^{2+}-triggered neurotransmitter release, *Cplx1* (complexin 1) and *Syt1* (synaptotagmin 1)[38, 39], were the 12th and 15th, respectively, most enriched genes in *Pomc*-negative ARC^{Vglut2} neurons relative to *Pomc*-positive ARC^{Vglut2} neurons. We then compared expression levels of these two genes by the *Pomc*-positive and *Pomc*-negative subsets of ARC^{Vglut2} neurons, as well as the expression levels of Vglut2 (*Slc17a6*), which confers capacity to synaptically release glutamate. Of interest, *Cplx1*, *Syt1* and Vglut2 gene expression were reduced in *Pomc*-positive versus *Pomc*-negative ARC^{Vglut2} neurons by 80%, 78% and 71%, respectively (Supplementary Fig. 4d). The much lower expression of *Cplx1, Syt1* and Vglut2, by *Pomc*-positive ARC^{Vglut2} neurons, compared with *Pomc*-negative ARC^{Vglut2} neurons, may explain their ineffective glutamatergic transmission onto PVH neurons. However, our results do not exclude the possibility that higher translational activity or greater protein stability could compensate for the lower transcript levels in *Pomc*-positive ARC^{Vglut2} neurons relative to *Pomc*-negative ARC^{Vglut2} neurons.

Glutamatergic ARC satiety neurons are marked by expression of the oxytocin receptor

Since a subset of ARC^{Vglut2} neurons is *Kiss1*-positive, we addressed whether ARC^{Kiss1} neurons regulate satiety. *Kiss1*-Cre mice[35] were used for this purpose. First, we injected AAV-DIO-ChR2 into the ARC and performed CRACM. Of note, we detected light-evoked EPSCs in a small subset (2/14) of ARC^{Kiss1}→uPVH neurons (Supplementary Fig. 5a), indicating that glutamatergic ARC^{Kiss1} afferents are a minority of the ARC^{Vglut2} neuron afferents to PVH. Next, we bilaterally transduced ARC^{Kiss1} neurons with AAV-DIO-hM3Dq (Supplementary Fig. 5b). CNO administration effectively activated hM3Dq-expressing ARC^{Kiss1} neurons as assessed by Fos induction (Supplementary Fig. 5c). Stimulation of ARC^{Kiss1} neurons, however, failed to rapidly suppress dark-cycle feeding (Supplementary Fig. 5d). Thus, ARC^{Kiss1} (as well as the ARC^{POMC}) neurons are not the subset that rapidly induces satiety.

Of interest, our RNA-seq analysis revealed that some ARC^{Vglut2} neurons express the gene encoding the oxytocin receptor (*Oxtr;* Fig. 5a). Notably, we failed to detect *Oxtr* expression in *Kiss1*-positive ARC^{Vglut2} neurons (Fig. 5a) or Vglut2-negative ARC neurons we profiled using single-cell RNA-Seq (unpublished data). Given these findings and a previous study demonstrating that intra-ARC injections of oxytocin rapidly suppresses feeding[40], we wondered whether ARC^{Oxtr} marks the subset of ARC^{Vglut2} neurons that rapidly induce satiety when stimulated. To further investigate ARC^{Oxtr} neurons, we obtained *Oxtr*-Cre mice[41]. Consistent with GENSAT's expression atlas, Cre activity was restricted to a small number of ARC neurons (Fig. 5b). Also, confirming our RNA-seq analysis, approximately 50% of ARC^{Oxtr} neurons expressed POMC as assessed by immunohistochemistry (Fig. 5b). To characterize the effect of oxytocin on ARC^{Oxtr} neurons, we recorded from fluorescently labeled cells in brain slices from *Oxtr*-Cre::tdTomato mice and found that bath-applied oxytocin markedly increased the firing rate of synaptically isolated ARC^{Oxtr} neurons (*i.e.*, in presence of CNQX, D-AP5 and bicuculline; Fig. 5c). Thus, *Oxtr*-Cre targets a small

population of ARC neurons that are directly activated by oxytocin. Some of these are a subset of ARC^{POMC} neurons while others are not.

Next, we probed connectivity of ARC^{Oxtr} neurons to unidentified PVH (uPVH) neurons. Following AAV-DIO-ChR2 delivery into the ARC of *Oxtr*-Cre mice, we detected light-evoked glutamatergic EPSCs in a subset (7/21) of $ARC^{Oxtr}\rightarrow$uPVH neurons (Fig. 5d). Given that the majority of ARC neurons are GABAergic[28], we also assessed if any PVH-projecting ARC^{Oxtr} neurons synaptically release GABA. Remarkably, we failed to detect light-evoked IPSCs in any of the $ARC^{Oxtr}\rightarrow$uPVH neurons tested (Supplementary Fig. 6a). Thus, no PVH-projecting ARC^{Oxtr} neurons are GABAergic. Given that ARC^{POMC} neurons are incapable of light-evoked synaptic release of glutamate in the PVH (Fig. 3a, b), these excitatory ARC^{OxtR} afferents must come from ARC^{Oxtr} neurons that lack POMC.

To assess the effect of ARC^{Oxtr} stimulation on dark-cycle feeding, we bilaterally transduced ARC^{OxtR} neurons with AAV-DIO-hM3Dq (Supplementary Fig. 6b). CNO administration effectively activated ARC^{Oxtr} neurons as assessed by Fos induction (Supplementary Fig. 6c). Of note, stimulation of ARC^{Oxtr} neurons rapidly suppressed dark-cycle feeding (Fig. 5e). In addition, stimulation of ARC^{Oxtr} neurons decreased refeeding in mice that were fasted for 24 hours (Supplementary Fig. 6d). To determine if the PVH is a downstream effector site for ARC^{OxtR} neurons, we optogenetically activated ChR2-expressing ARC^{Oxtr} terminals in the PVH (Fig. 5f). This terminal stimulation rapidly suppressed dark-cycle feeding (Fig. 5f and Supplementary Fig. 6e). Thus, as with hunger-promoting inhibitory ARC^{AgRP} neurons, the PVH is an important effector site for satiety-promoting glutamatergic ARC^{Oxtr} neurons.

Excitatory ARC^{Vglut2} and inhibitory ARC^{AgRP} projections synaptically converge on PVH^{MC4R} neurons

To see if glutamatergic ARC neurons, like ARC^{AgRP} neurons[23], preferentially engage PVH^{MC4R} neurons, we performed CRACM experiments using *Mc4r*-t2a-Cre mice[23]. In these studies, AAV-DIO-GFP was injected into the PVH to visualize PVH^{MC4R} neurons and Cre-independent AAV-Chr2 was injected into the ARC (see methods). Light evoked, AMPAR-mediated EPSCs could be detected in the majority (14/21) of $ARC^{Glutamatergic}\rightarrow PVH^{MC4R}$ neurons (Fig. 6a, d and Supplementary Fig. 7a). In contrast, only a small subset (1/7) of $ARC^{Glutamatergic}\rightarrow PVH^{MC4R\text{-}negative}$ neurons received light-evoked EPSCs (Fig. 6d and Supplementary Fig. 7b). Thus, $ARC^{Glutamatergic}$ neurons selectively engage PVH^{MC4R} neurons.

To test if ARC^{OxtR} neurons also preferentially engage PVH^{MC4R} neurons, we generated *Oxtr*-Cre::*Mc4r*-t2a-Cre mice. AAV-DIO-GFP was injected into the PVH to visualize PVH^{MC4R} neurons and AAV-DIO-ChR2-mCherry was injected into the ARC. We detected light-evoked EPSCs in the vast majority (17/20) of $ARC^{Oxtr}\rightarrow PVH^{MC4R}$ neurons (Fig. 6b, d) and, again only in a small subset (3/10) of $PVH^{MC4R\text{-}negative}$ neurons (Fig. 6d and Supplementary Fig. 7c). We also tested $ARC^{POMC}\rightarrow PVH^{MC4R}$ connectivity in *Pomc*-Cre::*Mc4r*-t2a-Cre mice. AAV-DIO-GFP was injected into the PVH to visualize PVH^{MC4R} and AAV-DIO-ChR2-mCherry was injected into the ARC. In agreement with our earlier results, we failed to detect light-evoked EPSCs in all but one PVH^{MC4R} neuron (Fig. 6c, d).

These CRACM studies demonstrate that, like ARC^{AgRP} neurons[23], excitatory ARC^{Oxtr} neurons, preferentially engage PVH^{MC4R} neurons.

Due to the high connectivity of both $ARC^{AgRP}\rightarrow PVH^{MC4R}$ (ref.[23]) and $ARC^{Oxtr}\rightarrow PVH^{MC4R}$ neurons (Fig. 6b, d), we reasoned that convergence of ARC^{AgRP} input and ARC^{Oxtr} input onto the same downstream PVH neurons was likely. To assess this possibility, we transduced both ARC^{AgRP} and ARC^{Oxtr} neurons in *Agrp*-IRES-Cre::*Oxtr*-Cre mice with AAV-DIO-ChR2 and recorded light-evoked IPSCs (ARC^{AgRP} input) and light-evoked EPSCs (ARC^{Oxtr} input) from the same downstream uPVH neurons. This was accomplished by alternating between the holding potential of 0 mV (ARC^{AgRP} input) and −70 mV (ARC^{Oxtr} input), respectively (Fig. 6e). Of 16 uPVH neurons tested, 2 received only ARC^{AgRP} input, 2 received only ARC^{Oxtr} input, and 6 received dual input from both (Fig. 6e). Thus, ARC^{AgRP} and ARC^{Oxtr} afferents often converge on single PVH neurons.

α-MSH post-synaptically increases glutamatergic transmission onto PVH^{MC4R} neurons

Given that PVH^{MC4R} neurons are a key downstream site for ARC^{Vglut2} neurons, we wondered if the fast acting glutamatergic and slow acting α-MSH satiety pathways interact via α-MSH-mediated effects on plasticity of excitatory inputs onto PVH^{MC4R} neurons. This possibility is of interest because i) ARC^{POMC} neurons heavily innervate the PVH where α-MSH promotes satiety[15, 16], and ii) α-MSH/MC4R action in other contexts can affect synaptic plasticity[42, 43]. To address this possibility, we recorded spontaneous excitatory postsynaptic currents (sEPSC) from PVH^{MC4R} neurons identified in *Mc4r*-t2a-Cre::tdTomato [Ai9 (Rosa26-CAG-loxSTOPlox-tdTomato)] mice and tested the affect of the POMC-derived MC4R agonist α-MSH on sEPSCs in PVH^{MC4R} neurons. We found that *ex vivo* treatment with α-MSH (250 nM)[42] markedly increased the number of large-amplitude sEPSCs and the mean amplitude of sEPSCs (Fig. 7a, b). In contrast, the frequency of sEPCSs in PVH^{MC4R} neurons was not affected by α-MSH (Fig. 7a, b). Given that the postsynaptic neurons express the MC4R, a receptor for α-MSH, this raises the important possibility that α-MSH potentiates glutamatergic transmission via a postsynaptic mechanism. Consistent with this, we found that α-MSH increased by 2-fold the ratio of the amplitude of electrically-evoked AMPAR- to N-methyl-D-aspartate receptor (NMDAR)-EPSCs (AMPAR/NMDAR ratio) – a measure of postsynaptic plasticity (Supplementary Fig. 8a). In contrast, we failed to detect changes in glutamate release probability by α-MSH treatment, as assessed by paired-pulse ratios (PPRs) of electrically-evoked EPSCs – further arguing against a presynaptic mechanism (Supplementary Fig. 8b).

We next determined if absence of endogenous α-MSH, *in vivo*, affects glutamatergic synaptic activity onto PVH^{MC4R} neurons. Towards these ends, we generated $Pomc^{lox/lox}$ mice (Supplementary Fig. 8c) and crossed them to *Mc4r*-t2a-Cre mice to generate $Pomc^{lox/lox}$::*Mc4r*-t2a-Cre mice. In these mice, *Pomc* deletion (POMC knock out; POMC KO) was achieved by delivery of AAV-Cre-mCherry into the ARC (Fig. 7c). Visualization of PVH^{MC4R} neurons was achieved by delivery of AAV-DIO-GFP into the PVH (Fig. 7c). AAV-Cre-mCherry effectively deleted POMC expression as revealed by POMC immunohistochemistry (Fig. 7c). We found that the number of large-amplitude sEPSCs and, consistent with this, the mean amplitude of sEPSCs in PVH^{MC4R} neurons in POMC KO

mice was markedly reduced (Fig. 7c, d). In contrast, we failed to detect changes in the frequency of sEPSCs in PVH^{MC4R} neurons in POMC KO mice (Fig. 7c, d). Together, these results demonstrate that α-MSH released by ARC^{POMC} neuron terminals postsynaptically augments glutamatergic synaptic activity in PVH^{MC4R} neurons.

To determine if glutamateric transmission across the $ARC^{Oxtr}\rightarrow PVH^{MC4R}$ synapse is specifically increased by α-MSH, we delivered AAV-DIO-ChR2-EYFP into the ARC of *Oxtr*-Cre::*Mc4r*-t2a-Cre::tdTomato mice and recorded light-evoked EPSCs from PVH^{MC4R} neurons (tdTomato-positive; Fig. 7e). We found that α-MSH significantly increased the AMPAR/NMDAR ratios of light-evoked EPSCs (Fig. 7f). In contrast, the PPRs of light-evoked EPSCs in $ARC^{Oxtr}\rightarrow PVH^{MC4R}$ neurons were not affected by α-MSH (Fig. 7g). These findings demonstrate that excitatory $ARC^{Oxtr}\rightarrow PVH^{MC4R}$ inputs are postsynaptically potentiated by α-MSH.

Discussion

Current models for homeostatic control of feeding lack a rapidly-acting ARC-based satiety mechanism that is temporally analogous to that provided by rapidly-acting, hunger-promoting ARC^{AgRP} neurons. In the present study we report the discovery of this missing component, namely glutamate-releasing neurons in the ARC that express the oxytocin receptor. We demonstrate that chemogenetic activation/inhibition of $ARC^{Vglut2/Oxtr}$ neurons, in contrast to ARC^{POMC} neurons, rapidly and robustly decreases/increases hunger, respectively. Furthermore, we show that the PVH is an important effector site for $ARC^{Vglut2/Oxtr}$ neurons. They project to and specifically induce EPSCs in PVH^{MC4R} neurons, and optogenetic stimulation of their terminals in the PVH rapidly decreases feeding. Using a “convergent CRACM” approach to simultaneously test for dual input, we show that $ARC^{Vglut2/Oxtr}$ satiety neurons and inhibitory ARC^{AgRP} hunger neurons converge onto the same downstream PVH^{MC4R} neurons (Supplemental Fig. 9). In contrast to the hunger-promoting system where slow- (AgRP) and rapid-acting signals (GABA and NPY) are conveyed by one group of neurons (ARC^{AgRP} neurons)[18, 24], the counteracting satiety-promoting system is split into two parallel-projecting neurons, the previously known ARC^{POMC} neurons which deliver slow-acting α-MSH, and the previously unknown $ARC^{Vglut2/Oxtr}$ neurons which release the rapid-acting transmitter, glutamate (Supplemental Fig. 9). Importantly, these two parallel-projecting satiety neurons interact as α-MSH released by ARC^{POMC} neurons postsynaptically increases glutamatergic transmission across the $ARC^{Vglut2/Oxtr}\rightarrow PVH^{MC4R}$ synapse (Supplemental Fig. 9). This missing rapid-acting component, working in concert with ARC^{POMC} neurons, provides the full “yang” to the ARC^{AgRP} neuron’s “yin”.

Many ARC^{POMC} neurons express glutamatergic (Vglut2) or GABAergic (GAD isoforms) markers[33, 34] suggesting that they are capable of synaptically releasing glutamate and/or GABA. Despite this, a recent study[26] established that $ARC^{POMC}\rightarrow PVH$ projections are largely ineffective in releasing glutamate or GABA in response to light/ChR2-evoked depolarization (light-evoked currents could be detected in only 3/66 of PVH neurons). In the present study, we confirm the ineffectiveness of synaptic transmission by $ARC^{POMC}\rightarrow PVH$ projections. Indeed, we observed no light/ChR2-evoked glutamatergic currents and no light/

ChR2-evoked GABAergic currents in all 71 PVH neurons sampled. In striking contrast, using Vglut2-IRES-Cre mice to express ChR2 in all ARC^{Vglut2} neurons, we observed light/ChR2-evoked glutamatergic currents in a substantial subset (40%) of PVH neurons. Thus, ARC^{Vglut2}→PVH projections, unlike ARC^{POMC}→PVH projections, are effective in rapid glutamatergic synaptic transmission. Since the PVH contains neurons that promote satiety[8, 19–24] and since PVH neurons efficiently integrate and summate excitatory synaptic inputs to control neuron excitability[27], we believe our findings to be significant, and suggest an important, unique role for glutamatergic transmission from POMC-negative ARC^{Vglut2} neurons. The reason why POMC-positive ARC^{Vglut2} PVH projections are ineffective in synaptic transmission is presently unknown, but could be related to their much lower expression of genes involved in fast, Ca^{2+}-triggered glutamate release[38, 39], *Vglut2*, *Syt1* and *Cplx1* (Supplementary Fig. 4).

It is noteworthy that ARC^{Vglut2} neurons express the oxytocin receptor and that Oxtr-Cre mice target glutamatergic ARC neurons that exert strong, rapid control over satiety. It has previously been established that exogenous administration of oxytocin acutely decreases food intake in mice[40], monkeys[44] and humans[45]. Given that i) acute suppression of feeding occurs with intra-ARC injection of oxytocin[40], ii) oxytocin exerts a direct stimulatory effect on ARC^{Oxtr} neurons and iii) ARC neurons are highly accessible to circulating factors, our finding provide a potential basis for the satiety-inducing effect of exogenously administered oxytocin. This possibility is of interest as oxytocin is being investigated as an anti-obesity drug[46]. Given their accessibility to circulating factors and that $ARC^{Vglut2/Oxtr}$ neurons exert hitherto unknown strong control over satiety, they may also provide neural mechanisms for other previously observed effects for which the basis is either unknown or incompletely understood – examples include but are not limited to regulation of satiety/hunger by cannabinoids or orally administered GLP-1R agonists. Further studies will be needed to address these possibilities.

Given that both ARC^{Vglut2} and ARC^{POMC} neurons project to the PVH, the site where hunger-suppressing MC4Rs reside[8, 22, 23], we examined how these two “parallel” satiety-promoting projections interact. While MC4R agonists are capable of directly increasing membrane potential and firing of PVH^{MC4R} neurons in *ex vivo* brain slices, the magnitude of these increases in PVH^{MC4R} neurons that project to the central lateral parabrachial nucleus (cLPBN), the downstream site through which PVH^{MC4R} neurons mediate satiety, is generally small[23]. This raises the possibility that the direct effect of αMSH/MC4Rs on neuron excitability plays a smaller role in regulating cLPBN-projecting PVH^{MC4R} neuron activity. Based on this, and importantly on the fact that opto- or chemogenetic stimulation of ARC^{POMC} neurons is unable to rapidly reduce feeding (Fig. 1 and refs. [4, 12, 17]), we suggest that ARC^{POMC} neurons do not work in isolation but instead decrease hunger by increasing the strength of excitatory synaptic transmission onto PVH^{MC4R} satiety neurons (Supplementary Fig. 9). Using an *ex vivo* CRACM approach, to selectively monitor the strength of $ARC^{Vglut2/Oxtr}$→PVH^{MC4R} synapses, we show that α-MSH postsynaptically upregulates glutamatergic transmission across this projection. This is consistent with two prior studies demonstrating that MC4Rs affect excitatory synaptic transmission via postsynaptic mechanisms – albeit in opposite directions depending upon cellular context[42, 43]. Our observation suggests that αMSH released by ARC^{POMC} neurons sets the

gain on ARC^{Vglut2} excitatory input to downstream PVH^{MC4R} satiety neurons – and hence satiety. This plasticity is likely important given that the vast majority of PVH^{MC4R} neurons receive functionally consequential monosynaptic excitatory input from ARC^{Vglut2} neurons. Thus, relevant "substrate" exists for αMSH/MC4R-mediated plasticity. Overall, our work provides a novel mechanism for α-MSH/MC4R regulation of satiety, namely plasticity of excitatory input onto PVH^{MC4R} neurons.

Online methods

Animals

All animal care and experimental procedures were approved by the National Institute of Health and Beth Israel Deaconess Medical Center Institutional Animal Care and Use Committee. Mice were housed at 22–24 °C with a 12 h light (06:00)/dark (18:00) cycle with standard mouse chow (Teklad F6 Rodent Diet 8664) and water provided *ad libitum*. *Pomc*-Cre[29], Vglut2-IRES-Cre[28], *Npy*-hrGFP[47], L10-GFP[25], *Agrp*-IRES-Cre[48], *Kiss1*-Cre[35], *Oxtr*-Cre[41], tdTomato[49], *Mc4r*-t2a-Cre[23] mice were maintained on a mixed background and have been described previously. All Cre driver and Cre-reporter mice were used in the heterozygous state. For all behavioral studies male mice between 8–12 weeks were used. For electrophysiological studies male and female mice between 5–12 weeks were used.

Generation of mice

***Pomc*-IRES-Cre mice—**Mice were generated using recombineering techniques as previously described[28]. Briefly, a selection cassette containing an internal ribosomal entry sequence (IRES) linked to Cre-recombinase and an Frt-flanked kanamycin resistance gene was targeted just downstream of the stop codon of the *Pomc* gene, so that Cre-recombinase expression was driven by the endogenous gene. A targeting plasmid containing the Cre-containing selection cassette and 4 kb genomic sequence upstream and downstream of the *Pomc* stop codon was isolated and used for embryonic stem cell targeting. Correctly targeted clones were identified by long range PCR and injected into blastocysts. Chimeric animals generated from blastocyst implantation were then bred for germline transmission of the altered *Pomc*-allele. Germline-expressing Flpe recombinase transgene mice[50] were then used to remove the neomycin selection cassette.

***Pomc*^{lox} mice—**A BAC clone containing the mouse *Pomc* genomic sequence was used to generate *Pomc*^{lox} mice using recombineering. To insert the first loxP sequence in intronic region between exon 2 and 3 located at ~922 bases downstream of the start codon, a PCR amplicon containing a loxP-kanamycin/neomycin-loxP cassette from the pSV-Cre plasmid was amplified with a forward primer containing 71 bp of *Pomc* homologous sequence upstream of the XhoI site and 19 bp of lox-kanamycin/neomycin-loxP and a reverse primer containing 71 bp of *Pomc* homologous sequence downstream of the XhoI site and 21 bp corresponding to the 3′ end of the lox-kanamycin/neomycin-loxP cassette. The PCR amplicon was transformed into electrocompetent EL350 bacteria that had been previously transfected with the *Pomc* BAC clone. Homologous recombination in the EL350 cells was induced as described previously[33] to insert the lox-kanamycin/neomycin-loxP cassette into the *Pomc* BAC at the XhoI site. The kanamycin/neomycin cassette was removed, leaving

behind one loxP sequence. The modified BAC was then transformed into EL250 bacteria, and the second loxP sequence was inserted at ~640 bases downstream of the stop codon by generating a second PCR amplicon containing a loxP-frt-kanamycin-frt cassette from the pL451 plasmid using a forward primer containing 70 bp of *Pomc* homologous sequence upstream of the SalI site and 19 bp of loxP-frtkanamycin-frt and a reverse primer containing 69 bp of *Pomc* homologous sequence downstream of the SalI site and 19 bp corresponding to the 3′ end of the loxP-frt-kanamycin-frt cassette. Homologous recombination was induced in the EL250 cells containing the modified *Pomc* BAC to insert the loxP-frtkanamycin-frt cassette into the SalI site and concomitant deletion of the restriction site. The targeting construct spanning ~4 kb upstream of the first loxP sequence and 4 kb downstream of the second loxP sequence was lifted out of the modified BAC and electroporated into W4 ES cells. Positively identified clones were injected into blastocysts, resulting in a number of 100% chimeric founders. The founders were bred to female mice bearing a germline-expressing Flpe recombinase transgene[50] to obtain germ-line transmission of the $Pomc^{lox}$ allele and to remove the frt-kanamycin-frt cassette.

Validation of *Pomc*-IRES-Cre mice

Pomc-IRES-Cre mice were crossed with tdTomato reporter mice. Cre activity in *Pomc*-IRES-Cre::tdTomato mice was highly restricted to the ARC, and was only seen in ARC^{POMC} neurons (Supplementary Fig. 1g, h). Thus, fidelity of Cre expression in *Pomc*-IRES-Cre mice is superior to *Pomc*-Cre BAC transgenic mice[51].

Brain tissue preparation

Animals were terminally anesthetized with 7% chloral hydrate diluted in saline (350 mg/kg) and transcardially perfused with phosphate-buffered saline (PBS) followed by 10% neutral buffered formalin (PFA). Brains were removed, stored in the same fixative for 2 hours, transferred into 20% sucrose at 4°C overnight, and cut into 30 μm sections on a freezing microtome (Leica) coronally into four equal series. A single series of sections per animal was used in the histological studies.

To determine the number of POMC-expressing ARC^{Vglut2} neurons, three sections, which covered the ARC, from each animal were used. POMC immunoreactive ARC^{Vglut2} cells from one hemisphere were manually counted. As previously reported, the expression level of *Slc17a6* (Vglut2) across the ARC[52] and in ARC^{POMC} neurons in particular[53] is not affected by fasting. These findings suggest that the number of POMC-expressing ARC^{Vglut2} neurons as reported here (Fig. 4b–d) is not affected by the fed/fasted state.

Immunohistochemistry

Brain sections were washed in PBS with Tween-20, pH 7.4 (PBST) and blocked in 3% normal donkey serum/PBST for 1 h at room temperature. Then, brain sections were incubated overnight at room temperature in blocking solution containing primary antiserum (rat anti-mCherry, Life Technologies M11217, 1:1,000; rabbit anti-POMC precursor, Phoenix Pharmaceuticals H-029-30, 1:3,000, goat anti-AgRP, Neuromics GT15023, 1:3,000, chicken anti-GFP, Life Technologies A10262, 1:1,000, goat anti-Fos, Calbiochem PC38, 1:1,000). The next morning sections were extensively washed in PBS and then incubated in

Alexa-fluorophore secondary antibody (Molecular Probes, 1:1,000) for 1 h at room temperature. After several washes in PBS, sections were mounted on gelatin-coated slides and fluorescence images were captured with Olympus VS120 slide scanner microscope.

Electrophysiology

Animals were deeply anesthetized, decapitated and brains were quickly removed into ice-cold cutting solution consisting of (in mM): 72 sucrose, 83 NaCl, 2.5 KCl, 1 NaH_2PO4, 26 $NaHCO_3$, 22 glucose, 5 $MgCl_2$, 1 $CaCl_2$, oxygenated with 95% O_2/5% CO_2, measured osmolarity 310 – 320 mOsm/l. 300-μm-thick coronal sections were cut with a Leica VT1000S vibratome and incubated in oxygenated cutting solution at 34 °C for 45 min. Slices were transferred to oxygenated aCSF (126 mM NaCl, 21.4 mM $NaHCO_3$, 2.5 mM KCl, 1.2 mM NaH_2PO_4, 1.2 mM $MgCl_2$, 2.4 mM $CaCl_2$, 10 mM glucose) and stored in the same solution at room temperature (20–24 °C) for at least 60 min prior to recording. A single slice was placed in the recording chamber where it was continuously superfused at a rate of 3–4 ml per min with oxygenated aCSF. Neurons were visualized with an upright microscope (SliceScope, Scientifica) equipped with infrared-differential interference contrast and fluorescence optics. Borosilicate glass microelectrodes (5–7 MΩ) were filled with internal solution.

Loose-seal, cell-attached recordings (seal resistance, 20–50 MΩ) were made in voltage clamp mode with aCSF as internal solution and holding current maintained at V_h = 0 mV.

To assess the effect of CNO on hM3Dq-expressing ARC^{POMC} neurons, 5- to 7-week-old *Pomc*-Cre mice were injected with AAV8-DIO-hM3Dq-mCherry into the ARC 2–3 weeks before recording. To assess the effect of CNO on hM4Di-expressing ARC^{Vglut2} neurons, 5- to 7-week-old Vglut2-IRES-Cre mice were injected with AAV8-DIO-hM4Di-mCherry into the ARC 2–3 weeks before recording. After acquisition of stable loose-seal cell-attached recordings for 3–5 min, aCSF solution containing CNO (10 μM) was perfused into the brain slice preparation.

To assess the effect of oxytocin on ARC^{Oxtr} neurons, loose-seal cell-attached recordings were performed on fluorescently labeled ARC cells in *Oxtr*-Cre::tdTomato mice. CNQX (10 μM), D-AP5 (50 μM) and bicuculline (10 μM) were added to the aCSF to synaptically isolate ARC^{Oxtr} neurons. After acquisition of stable recordings for 3–5 min, aCSF solution containing oxytocin (200 nM) was perfused into the brain slice preparation.

To assess effects of fasting on ARC^{Vglut2} neurons, recordings were performed on fluorescently labeled ARC cells in Vglut2-IRES-Cre::L10-GFP mice. Two groups of animals were provided with fresh cages 24 hours prior to euthanasia. The fed group had ad libitum access to food, while no food was provided to the fasted group.

sIPSCs in ARC^{Vglut2} neurons were recorded in whole-cell voltage-clamp mode, with membrane potential clamped at V_h = −70 mV using a CsCl-based internal solution consisting of (in mM): 140 CsCl, 1 BAPTA, 10 HEPES, 5 $MgCl_2$, 2 Mg-ATP, and 0.3 Na_2-GTP (pH 7.35 adjusted with NaOH; 295 mOsm · kg^{-1}) in presence of D-AP5 and CNQX.

For CRACM experiments, recordings were obtained using a Cs^+-based low Cl^- internal solution consisting of (in mM): 135 $CsMeSO_3$, 10 HEPES, 1 EGTA, 4 $MgCl_2$, 4 Na_2-ATP, 0.4 Na_2-GTP, 10 Na_2-phosphocreatine (pH 7.3 adjusted with CsOH; 295 mOsm · kg^{-1}; E_{Cl} = −70 mV). Light-evoked EPSCs and IPSCs were recorded in whole-cell voltage-clamp mode, with membrane potential clamped at V_h = −70 mV and 0 mV, respectively. CNQX and D-AP5 or bicuculline were included to isolate glutamatergic/GABAergic currents. The light-evoked EPSC/IPSC detection protocol consisted of four blue light pulses (473 nm wavelength, 5 msec) administered 1 s apart during the first 4 s of an 8-s sweep, repeated for a total of 30 sweeps. Evoked EPSCs/IPSCs with short latency (≤6 ms) upon light stimulation were considered as light-driven. As discussed by others, such currents are most likely monosynaptic[31]. Number of animals used for CRACM experiments: $ARC^{AgRP}\rightarrow ARC^{Vglut2}$, n = 3; ARC^{POMC} (*Pomc*-Cre)→uPVH, n = 2; ARC^{POMC} (*Pomc*-IRES-Cre)→uPVH, n = 5; $ARC^{Vglut2}\rightarrow$uPVH, n = 2; $ARC^{Kiss1}\rightarrow$uPVH, n = 2; $ARC^{Oxtr}\rightarrow$uPVH, n = 2; $ARC^{Glutamatergic}\rightarrow PVH^{MC4R}$ or $PVH^{MC4R\text{-}negative}$, n = 2; $ARC^{POMC}\rightarrow PVH^{MC4R}$, n = 2; $ARC^{Oxtr}\rightarrow PVH^{MC4R}$ or $PVH^{MC4R\text{-}negative}$, n = 2.

For CRACM experiments in which recordings were made from PVH^{MC4R} neurons, the PVH^{MC4R} neurons were labeled with AAV8-DIO-GFP injected into the PVH of *Mc4r*-t2a-Cre mice (Fig. 6a, Supplementary Fig. 7a, b), *Oxtr*-Cre::*Mc4r*-t2a-Cre (Fig. 6b, Supplementary Fig. 8c) or *Pomc*-Cre::*Mc4r*-t2a-Cre (Fig. 6c). For these experiments mCherry-tagged ChR2 was used. The Vglut2-IRES-Cre allele could not be used to selectively express ChR2 in ARC^{Vglut2} neurons (Fig. 6a and Supplementary Fig. 7a, b) since most neurons in the PVH express Vglut2 and Cre activity from the *Mc4r*-t2a-Cre allele is necessary to selectively visualize PVH^{MC4R} neurons. Instead, ARC neurons were transduced with Cre-independent AAV-ChR2-mCherry and synaptic blockers were used to isolate glutamatergic EPSCs. Note that no Cre activity could be detected in the PVH of *Oxtr*-Cre mice. Thus, Cre activity from the *Mc4r*-t2a-Cre allele visualized PVH^{MC4R} neurons in *Oxtr*-Cre::*Mc4r*-t2a-Cre mice transduced with AAV-DIO-GFP (Fig. 6b and Supplementary Fig. 7c) or in *Oxtr*-Cre::*Mc4r*-t2a-Cre::tdTomato (Fig. 7e–g) mice. As previously reported[23], no Cre activity could be detected in the ARC of *Mc4r*-t2a-Cre::tdTomato *mice.*

For monitoring α-MSH-induced synaptic changes, recordings were performed on fluorescently labeled PVH cells in *Mc4r*-t2a-Cre::tdTomato mice. Brain slices were incubated in aCSF containing α-MSH (250 nM) for at least 2–3 h at room temperature (20–24°C) before recordings were made. Acute application of α-MSH during recordings failed, on average, to affect sEPSC amplitude or frequency during 12 min of application. For all experiments examining the effects of α-MSH incubation, recordings from control cells kept in aCSF were interleaved with recordings from cells undergoing α-MSH treatment.

Spontaneous EPSCs (sEPSCs) and electrically-evoked EPSCs were recorded at V_h = −70 mV using a Cs^+-based internal solution (see above) in presence of bicuculline. A patch pipette filled with aCSF was placed within 20–40 μm from the cell body of the patched neuron, and EPSCs were evoked electrically by single monopolar square pulse stimulation. Test pulses of 0.1 ms duration (150 – 400 μA) were given at intervals of 15 s. Paired-pulse ratios (PPRs) of electrically-evoked EPSCs were obtained by applying a pair of synaptic stimuli 50 ms apart. PPRs of light-evoked EPSCs were recorded at V_h = −70 mV and

obtained by applying a pair of light stimuli 100 ms apart. PPRs were determined by dividing the amplitude of the second EPSC by the amplitude of the first EPSC averaged over 5 min epochs of 20 EPSCs.

AMPAR/NMDAR ratios were recorded using an internal solution consisting of (in mM): 135 $CsMeSO_3$, 10 HEPES, 0.2 EGTA, 4 $MgCl_2$, 4 Na_2-ATP, 0.4 Na_2-GTP, 10 TEA, 0.1 spermine (pH 7.3 adjusted with CsOH; 295 mOsm · kg^{-1}) in presence of bicuculline. Electrically-evoked AMPAR/NMDAR ratios were recorded at V_h = +40 mV and AMPAR-mediated EPSCs were isolated by adding D-AP5 to block NMDAR–mediated synaptic currents. The NMDAR-mediated EPSCs were calculated by subtracting the AMPAR-mediated EPSCs from the EPSCs measured in the absence of D-AP5. The electrically-evoked AMPAR/NMDAR ratios were calculated by dividing the peak amplitudes. Light-evoked AMPAR/NMDAR ratios were recorded in presence of bicuculline and were calculated as the ratio of the peak amplitude of the light-evoked EPSC at V_h = −70 mV (AMPAR-mediated EPSCs) to the magnitude of the light-evoked EPSC recorded at V_h = +40 mV at 25–50 ms after light stimulation (NMDAR-mediated EPSCs). Access resistance (<30 MΩ) was continuously monitored by a voltage step and recordings were accepted for analysis if changes were <15%.

All recordings were made using a Multiclamp 700B amplifier, and data were filtered at 2 kHz and digitized at 10 kHz. To photostimulate channelrhodopsin2-positive fibers, a laser or LED light source (473 nm) was used. The blue light was focused onto the back aperture of the microscope objective, producing wide-field exposure around the recorded cell of 10–15 mW per mm^2. The light power at the specimen was measured using an optical power meter PM100D (Thorlabs). The light output was controlled by a programmable pulse stimulator, Master-8 (A.M.P.I.) and pClamp 10.2 software (Axon Instruments). All recordings were analyzed offline using Clampfit 10.

Single-cell RNA-seq

Single-cell RNA sequencing was performed as previously described[23]. Briefly, ARC^{Vglut2} neurons were identified based on their fluorescence (GFP-positive in Vglut2-IRES-Cre::L10-GFP mice). Brain slices were sectioned as for electrophysiological experiments (see above) and the ARC was micro-dissected, and dissociated with papain. Individual GFP-positive ARC cells were isolated from suspension by micropipette, then washed, frozen at −80 °C, and lysed for cDNA synthesis and PCR amplification. To control for mRNA contamination during cell picking, an equivalent volume of cell-picking buffer was sampled and processed with each batch of single-cell samples. Amplified cDNA was analyzed by quantitative PCR (qPCR) for expression of the housekeeping gene expression, Actb. Single-cell samples showing low or undetectable levels of Actb expression were excluded from further use, as were batches of samples in which the cell-picking buffer showed evidence of mRNA contamination (i.e., *Actb*-positive). Barcoded RNA-seq libraries were constructed with a commercially available kit (Ovation Rapid Library Kit NuGen, California, USA) and sequenced in multiplex by Illumina HiSeq (50-base single-end reads). Pass-filter reads were aligned to the mouse genome (mm10) and quantified by TopHat/Bowtie2/Cufflinks software in units of RPKM (reads per kilobase exon per million fragments mapped).

Cluster analysis

Each of the 23 ARC^{Vglut2} neurons was represented by the expression of 90 neuropeptide genes (Supplemental table 1). Of the 92 neuropeptide genes provided (gene list from www.neuropeptides.nl[54]), we excluded *Oxt* and *Avp* from our analysis due to cross-contamination. To cluster the neurons to groups we first reduced the representation of each neuron to 3 dimensions. Dimensionality reduction was performed with the tSNE algorithm, using free and open source software written in Matlab (distributed under the FreeBSD License. https://lvdmaaten.github.io/tsne/). The software first performs a dimensionality reduction using standard Matlab principal component analysis. The first 10 principal components for each neuron were then fed into the tSNE procedure (with perplexity parameter set to 2). Following this procedure each neuron was represented by 3 tSNE dimensions. Next, we performed clustering using 'kmeans' procedure to find the four major groups. All analysis was done in Matlab.

Viral injections

Stereotaxic injections were performed using previously described procedures[23]. Mice were anesthetized with xylazine (5 mg per kg) and ketamine (75 mg per kg) diluted in saline (0.9%) and placed into a stereotaxic apparatus (KOPF). For postoperative care, mice were injected intraperitoneally with meloxicam (0.5 mg per kg). A micromanipulator (Grass Technologies, model S48 stimulator) was used to deliver the viruses at 2–5 nl per min and the pipette was withdrawn 5 min after injection. AAV1-FLEX-ChR2(H134R)-mCherry, AAV9-FLEX-ChR2(H134R)-EYFP, AAV9-CAG-ChR2(H134R)-mCherry (University of Pennsylvania School of Medicine), AAV8-DIO-hM3Dq-mCherry, AAV8-DIO-hM4Di-mCherry, AAV8-hSyn-mCherry-Cre, AAV5-hSyn-mCherry (University of North Carolina Vector Core), AAV8-DIO-synaptophysin-mCherry (Virovek, Inc) were injected into the ARC (coordinates, bregma: AP: −1.35 mm, DV: −6.00 mm, ML: ±0.2 mm). Mice with 'missed' injections, incomplete 'hits' or expression outside the ARC were excluded from analysis after post hoc examination of mCherry/GFP expression. AAV8-DIO-GFP (University of North Carolina Vector Core) was injected into the PVH (coordinates, bregma: AP: −0.75 mm, DV: −4.85 mm, ML: −0.20 mm).

Optic fiber implantation

Fiber implantation was performed using previously described procedures[23]. Optical fibers (200 μm diameter core; Thor Labs) were implanted unilaterally over the PVH (coordinates, bregma: AP: −0.70 mm, DV: −4.35 mm, ML: 0 mm). Fibers were fixed to the skull using dental acrylic and mice were allowed 2 weeks for recovery before acclimatization to the recording chambers for 1 week.

Food intake studies

All animals were singly housed for at least 2.5 weeks following surgery and handled for 10 consecutive days before the assay to acclimate mice to the experimental procedure. Feeding studies were performed in home cages with *ad libitum* food access to chow. The day before the experiment, mice were provided with fresh cages to avoid leftover of food spilling in the bedding. CNO was administered at 1 mg per kg of body weight. Saline was delivered at the

same volume to maintain consistency in the studies. Mice with 'missed' injections, incomplete 'hits' or expression outside the ARC were excluded from analysis after post hoc examination of mCherry expression.

For light-cycle measurements, animals were injected with either saline or CNO at 9:00 AM and food intake was monitored 1, 2, 3 and 4 h after i.p. injection from 9:00 AM to 1:00 PM. For refeeding experiments, mice were provided with fresh cages at 9:00 AM the day prior the experiment and no food was provided. Following 24 hour fasting, mice were injected with either saline or CNO at 8:45 the following day and food intake was monitored 1, 2, 3 and 4 h after i.p. injection from 9:00 AM to 1:00 PM. For dark-cycle measurements, animals were injected with either saline or CNO at 6:00 PM and food intake was monitored 1, 2, 3 and 4 h after i.p. injection from 6:00 PM to 10:00 PM. For 24 and 48 hours food intake measurements, animals were injected with either saline or CNO three times per day.

For *in vivo* optogenetic studies, fiber optic cables were firmly attached to the implanted fiber optic cannulae with zirconia sleeves. Light pulse trains (5 ms pulses of 20 Hz; 3 s on, 1 s off) were programmed using a waveform generator that provided input to a blue light LED (473 nm). The light power exiting the fiber optic cable was adjusted so that it had 5–8 mW measured using an optical power meter. After completion of photostimulation experiments, mice were perfused and the approximate locations of fiber tips were identified.

iBAT temperature

iBAT temperature was measured using a previously described method[55]. Temperature transponders (IPTT-300, Bio Medic Data Systems) were implanted subcutaneously above the iBAT pad between the scapula under anesthesia. Animals were allowed 1 week recovery and acclimation was performed with saline injection for 5 consecutive days. Data were collected using a handheld reader system (DAS-7006/7r; Bio Medic Data System) at time points indicated.

Statistical analysis

Statistical analyses were performed using Prism 6.0 (GraphPad) software. No statistical method was used to predetermine sample size. Sample sizes were chosen similar to those reported in previous publications[13, 23, 25, 28]. Randomization and blinding methods were not used. All data presented met the assumptions of the statistical test employed. Experimental animals were excluded if histological validation of the injection site demonstrated absence of reporter expression. This was established prior to data collection. N values represent final number of validated animals. For examining differences in the distribution of sEPSC amplitudes, we used MATLAB (Mathworks) to generate normalized frequency distributions and compared them using a Kolmogorov-Smirnov test.

Supplementary Material

Refer to Web version on PubMed Central for supplementary material.

Acknowledgments

This research was funded by the following NIH grants to B.B.L.: R01 DK075632, R01 DK096010, R01 DK089044, P30 DK046200, P30 DK057521; to J.M.R.: F32 DK103387; to J.N.C., AHA Postdoctoral Fellowship 14POST20100011. Y.M. was supported by a Charles A. King postdoctoral fellowship. Y.L. was supported by an EMBO postdoctoral fellowship. We thank members of B.B.L. lab for helpful discussions.

References

1. Langlet F. Tanycytes: a gateway to the metabolic hypothalamus. J Neuroendocrinol. 2014; 26:753–760. [PubMed: 25131689]
2. Rodriguez EM, Blazquez JL, Guerra M. The design of barriers in the hypothalamus allows the median eminence and the arcuate nucleus to enjoy private milieus: the former opens to the portal blood and the latter to the cerebrospinal fluid. Peptides. 2010; 31:757–776. [PubMed: 20093161]
3. Xu AW, et al. Effects of hypothalamic neurodegeneration on energy balance. PLoS Biol. 2005; 3:e415. [PubMed: 16296893]
4. Zhan C, et al. Acute and Long-Term Suppression of Feeding Behavior by POMC Neurons in the Brainstem and Hypothalamus, Respectively. J Neurosci. 2013; 33:3624–3632. [PubMed: 23426689]
5. Krude H, et al. Severe early-onset obesity, adrenal insufficiency and red hair pigmentation caused by POMC mutations in humans. Nat Genet. 1998; 19:155–157. [PubMed: 9620771]
6. Yaswen L, Diehl N, Brennan MB, Hochgeschwender U. Obesity in the mouse model of pro-opiomelanocortin deficiency responds to peripheral melanocortin. Nat Med. 1999; 5:1066–1070. [PubMed: 10470087]
7. Huszar D, et al. Targeted disruption of the melanocortin-4 receptor results in obesity in mice. Cell. 1997; 88:131–141. [PubMed: 9019399]
8. Balthasar N, et al. Divergence of melanocortin pathways in the control of food intake and energy expenditure. Cell. 2005; 123:493–505. [PubMed: 16269339]
9. Vaisse C, Clement K, Guy-Grand B, Froguel P. A frameshift mutation in human MC4R is associated with a dominant form of obesity. Nat Genet. 1998; 20:113–114. [PubMed: 9771699]
10. Yeo GS, et al. A frameshift mutation in MC4R associated with dominantly inherited human obesity. Nat Genet. 1998; 20:111–112. [PubMed: 9771698]
11. Luquet S, Perez FA, Hnasko TS, Palmiter RD. NPY/AgRP neurons are essential for feeding in adult mice but can be ablated in neonates. Science. 2005; 310:683–685. [PubMed: 16254186]
12. Aponte Y, Atasoy D, Sternson SM. AGRP neurons are sufficient to orchestrate feeding behavior rapidly and without training. Nat Neurosci. 2011; 14:351–355. [PubMed: 21209617]
13. Krashes MJ, et al. Rapid, reversible activation of AgRP neurons drives feeding behavior in mice. J Clin Invest. 2011; 121:1424–1428. [PubMed: 21364278]
14. Myers MG Jr, Olson DP. Central nervous system control of metabolism. Nature. 2012; 491:357–363. [PubMed: 23151578]
15. Morton GJ, Meek TH, Schwartz MW. Neurobiology of food intake in health and disease. Nat Rev Neurosci. 2014; 15:367–378. [PubMed: 24840801]
16. Gautron L, Elmquist JK, Williams KW. Neural control of energy balance: translating circuits to therapies. Cell. 2015; 161:133–145. [PubMed: 25815991]
17. Koch M, et al. Hypothalamic POMC neurons promote cannabinoid-induced feeding. Nature. 2015; 519:45–50. [PubMed: 25707796]
18. Krashes MJ, Shah BP, Koda S, Lowell BB. Rapid versus delayed stimulation of feeding by the endogenously released AgRP neuron mediators GABA, NPY, and AgRP. Cell Metab. 2013; 18:588–595. [PubMed: 24093681]
19. Bagnol D, et al. Anatomy of an endogenous antagonist: relationship between Agouti-related protein and proopiomelanocortin in brain. J Neurosci. 1999; 19:RC26. [PubMed: 10479719]
20. Cowley MA, et al. Integration of NPY, AGRP, and melanocortin signals in the hypothalamic paraventricular nucleus: evidence of a cellular basis for the adipostat. Neuron. 1999; 24:155–163. [PubMed: 10677034]

21. Giraudo SQ, Billington CJ, Levine AS. Feeding effects of hypothalamic injection of melanocortin 4 receptor ligands. Brain Res. 1998; 809:302–306. [PubMed: 9853124]
22. Shah BP, et al. MC4R-expressing glutamatergic neurons in the paraventricular hypothalamus regulate feeding and are synaptically connected to the parabrachial nucleus. Proc Natl Acad Sci U S A. 2014; 111:13193–13198. [PubMed: 25157144]
23. Garfield AS, et al. A neural basis for melanocortin-4 receptor-regulated appetite. Nat Neurosci. 2015; 18:863–871. [PubMed: 25915476]
24. Atasoy D, Betley JN, Su HH, Sternson SM. Deconstruction of a neural circuit for hunger. Nature. 2012; 488:172–177. [PubMed: 22801496]
25. Krashes MJ, et al. An excitatory paraventricular nucleus to AgRP neuron circuit that drives hunger. Nature. 2014; 507:238–242. [PubMed: 24487620]
26. Atasoy D, et al. A genetically specified connectomics approach applied to long-range feeding regulatory circuits. Nat Neurosci. 2014; 17:1830–1839. [PubMed: 25362474]
27. Branco T, et al. Near-Perfect Synaptic Integration by Nav1.7 in Hypothalamic Neurons Regulates Body Weight. Cell. 2016; 165:1749–1761. [PubMed: 27315482]
28. Vong L, et al. Leptin action on GABAergic neurons prevents obesity and reduces inhibitory tone to POMC neurons. Neuron. 2011; 71:142–154. [PubMed: 21745644]
29. Balthasar N, et al. Leptin receptor signaling in POMC neurons is required for normal body weight homeostasis. Neuron. 2004; 42:983–991. [PubMed: 15207242]
30. Atasoy D, Aponte Y, Su HH, Sternson SM. A FLEX switch targets Channelrhodopsin-2 to multiple cell types for imaging and long-range circuit mapping. J Neurosci. 2008; 28:7025–7030. [PubMed: 18614669]
31. Petreanu L, Huber D, Sobczyk A, Svoboda K. Channelrhodopsin-2-assisted circuit mapping of long-range callosal projections. Nat Neurosci. 2007; 10:663–668. [PubMed: 17435752]
32. Hahn TM, Breininger JF, Baskin DG, Schwartz MW. Coexpression of Agrp and NPY in fasting-activated hypothalamic neurons. Nat Neurosci. 1998; 1:271–272. [PubMed: 10195157]
33. Jarvie BC, Hentges ST. Expression of GABAergic and glutamatergic phenotypic markers in hypothalamic proopiomelanocortin neurons. J Comp Neurol. 2012; 520:3863–3876. [PubMed: 22522889]
34. Wittmann G, Hrabovszky E, Lechan RM. Distinct glutamatergic and GABAergic subsets of hypothalamic pro-opiomelanocortin neurons revealed by in situ hybridization in male rats and mice. J Comp Neurol. 2013; 521:3287–3302. [PubMed: 23640796]
35. Cravo RM, et al. Characterization of Kiss1 neurons using transgenic mouse models. Neuroscience. 2011; 173:37–56. [PubMed: 21093546]
36. Picelli S, et al. Smart-seq2 for sensitive full-length transcriptome profiling in single cells. Nat Methods. 2013; 10:1096–1098. [PubMed: 24056875]
37. Usoskin D, et al. Unbiased classification of sensory neuron types by large-scale single-cell RNA sequencing. Nat Neurosci. 2015; 18:145–153. [PubMed: 25420068]
38. Sudhof TC. Neurotransmitter release: the last millisecond in the life of a synaptic vesicle. Neuron. 2013; 80:675–690. [PubMed: 24183019]
39. Blakely RD, Edwards RH. Vesicular and plasma membrane transporters for neurotransmitters. Cold Spring Harb Perspect Biol. 2012; 4
40. Maejima Y, et al. Oxytocinergic circuit from paraventricular and supraoptic nuclei to arcuate POMC neurons in hypothalamus. FEBS Lett. 2014; 588:4404–4412. [PubMed: 25448678]
41. Nakajima M, Gorlich A, Heintz N. Oxytocin modulates female sociosexual behavior through a specific class of prefrontal cortical interneurons. Cell. 2014; 159:295–305. [PubMed: 25303526]
42. Lim BK, Huang KW, Grueter BA, Rothwell PE, Malenka RC. Anhedonia requires MC4R-mediated synaptic adaptations in nucleus accumbens. Nature. 2012; 487:183–189. [PubMed: 22785313]
43. Shen Y, Fu WY, Cheng EY, Fu AK, Ip NY. Melanocortin-4 receptor regulates hippocampal synaptic plasticity through a protein kinase A-dependent mechanism. J Neurosci. 2013; 33:464–472. [PubMed: 23303927]

44. Blevins JE, et al. Chronic oxytocin administration inhibits food intake, increases energy expenditure, and produces weight loss in fructose-fed obese rhesus monkeys. Am J Physiol Regul Integr Comp Physiol. 2015; 308:R431–438. [PubMed: 25540103]
45. Lawson EA, et al. Oxytocin reduces caloric intake in men. Obesity (Silver Spring). 2015; 23:950–956. [PubMed: 25865294]
46. Blevins JE, Baskin DG. Translational and therapeutic potential of oxytocin as an anti-obesity strategy: Insights from rodents, nonhuman primates and humans. Physiol Behav. 2015; 152:438–449. [PubMed: 26013577]
47. van den Pol AN, et al. Neuromedin B and gastrin-releasing peptide excite arcuate nucleus neuropeptide Y neurons in a novel transgenic mouse expressing strong Renilla green fluorescent protein in NPY neurons. J Neurosci. 2009; 29:4622–4639. [PubMed: 19357287]
48. Tong Q, Ye CP, Jones JE, Elmquist JK, Lowell BB. Synaptic release of GABA by AgRP neurons is required for normal regulation of energy balance. Nat Neurosci. 2008; 11:998–1000. [PubMed: 19160495]
49. Madisen L, et al. A robust and high-throughput Cre reporting and characterization system for the whole mouse brain. Nat Neurosci. 2010; 13:133–140. [PubMed: 20023653]
50. Farley FW, Soriano P, Steffen LS, Dymecki SM. Widespread recombinase expression using FLPeR (flipper) mice. Genesis. 2000; 28:106–110. [PubMed: 11105051]
51. Padilla SL, Reef D, Zeltser LM. Defining POMC neurons using transgenic reagents: impact of transient Pomc expression in diverse immature neuronal populations. Endocrinology. 2012; 153:1219–1231. [PubMed: 22166984]
52. Jovanovic Z, Tung YC, Lam BY, O'Rahilly S, Yeo GS. Identification of the global transcriptomic response of the hypothalamic arcuate nucleus to fasting and leptin. J Neuroendocrinol. 2010; 22:915–925. [PubMed: 20553370]
53. Henry FE, Sugino K, Tozer A, Branco T, Sternson SM. Cell type-specific transcriptomics of hypothalamic energy-sensing neuron responses to weight-loss. Elife. 2015; 4
54. Burbach JP. Neuropeptides from concept to online database http://www.neuropeptides.nl. Eur J Pharmacol. 2010; 626:27–48. [PubMed: 19837055]
55. Kong D, et al. GABAergic RIP-Cre neurons in the arcuate nucleus selectively regulate energy expenditure. Cell. 2012; 151:645–657. [PubMed: 23101631]

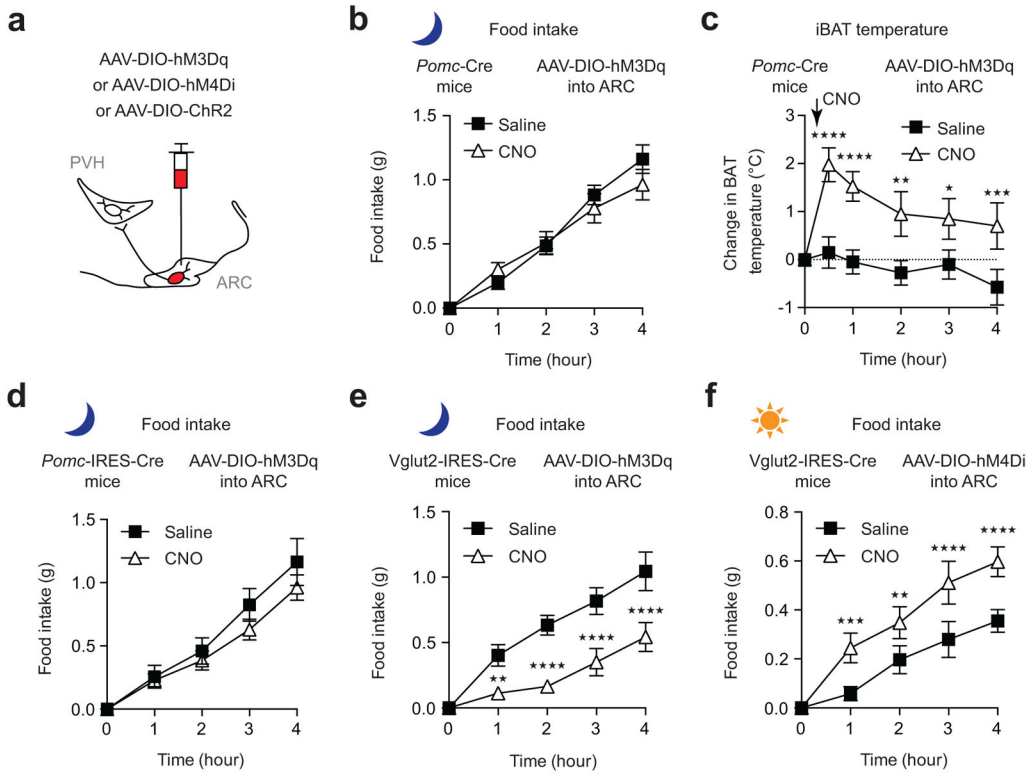

Figure 1. Regulation of feeding by ARC^{POMC} versus ARC^{Vglut2} neurons

a, Experimental schematic. **b, d, e,** Effect of CNO/hM3Dq stimulation of ARC^{POMC} neurons (**b**, **d**) or ARC^{Vglut2} neurons (**e**) on dark-cycle feeding. **c**, Effect of CNO/hM3Dq stimulation of ARC^{POMC} neurons on iBAT temperature. **f**, Effect of CNO/hM4Di inhibition of ARC^{Vglut2} neurons on light-cycle feeding. **b–f**, Data are presented as mean ± SEM. Mice from multiple litters. Repeated measures two-way ANOVA followed by Sidak's multiple comparisons test (**b**, $n = 5$ animals; Treatment F(1,4) = 0.3265, $P = 0.5983$; time F(4,16) = 89.82, $P < 0.0001$; interaction F(4,16) = 3.037, $P = 0.0485$. 1h, $P = 0.4831$; 2h, $P = 0.9980$; 3h, $P = 0.4831$; 4h, $P = 0.0610$; **c**, $n = 4$ animals. Treatment F(1,3) = 8.931, $P = 0.0582$; time F(5,15) = 8.008, $P = 0.0008$; interaction F(5, 15) = 6.494, $P = 0.0021$. 30 min, ****$P <$ 0.0001; 1h, ****$P < 0.0001$; 2h, **$P = 0.0011$; 3h, *$P = 0.0102$; 4h, ***$P = 0.0008$; **d**, $n = 4$ animals; Treatment F(1,3) = 0.7301, $P = 0.4557$; time F(4,12) = 75.69, $P < 0.0001$; interaction F(4, 12) = 1.475, $P = 0.2703$; **e**, $n = 4$ animals. Treatment F(1,3) = 63.28, $P =$ 0.0041; time F(4,12) = 40.61, $P < 0.0001$; interaction F(4, 12) = 10.40, $P = 0.0007$. 1h, **P = 0.0040; 2h, ****$P < 0.0001$; 3h, ****$P < 0.0001$; 4h, ****$P < 0.0001$; **f**, $n = 6$ animals. Treatment F(1,5) = 16.55, $P = 0.0096$; time F(4,20) = 24.66, $P < 0.0001$; interaction F(4, 20) = 7.808, $P = 0.0006$. 1h, ***$P = 0.0002$; 2h, **$P = 0.0016$; 3h, ****$P < 0.0001$; 4h, ****$P <$ 0.0001).

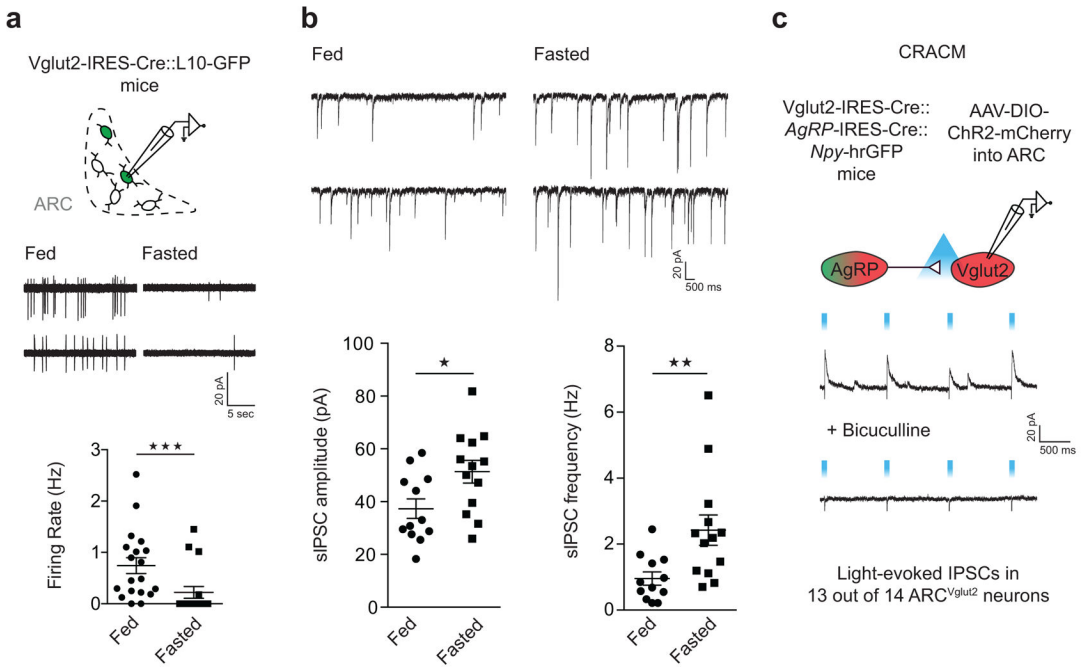

Figure 2. Effects of fasting on ARC^{Vglut2} neurons and their inhibition by ARC^{AgRP} neuron afferents

a, Top, schematic shows experimental approach used in (**a**) and (**b**). **a**, Representative traces (middle) and summary (bottom) of fasting effects on the firing rate of ARC^{Vglut2} neurons as assessed using cell-attached recordings. Number of animals: Fed/fasted, $N = 3/3$. Sample size (cells): Fed/fasted, $n = 19/17$; Fed (M = 0.7437, s.d. = 0.6771) versus fasted (M = 0.2208, s.d. = 0.4725): Two-tailed Mann-Whitney test: U = 61, ***$P = 0.0007$. **b**, Representative traces (top) and summary (bottom) of fasting effects on sIPSCs in ARC^{Vglut2} neurons. Number of animals, fed/fasted, $N = 3/3$; sample size (cells), fed/fasted, n = 12/13. Unpaired two-tailed t-test: sIPSC amplitude: Fed (M = 37.33, s.d. = 12.95) versus fasted (M = 51.34, s.d. = 15.5): t(23) = 2.442, *$P = 0.0227$; sIPSC frequency: Fed (M = 0.9563, s.d. = 0.6858) versus fasted (M = 2.423, s.d. = 1.667): t(23) = 2.830, **$P = 0.0095$. Data are presented as mean ± SEM**. c**, ARC^{AgRP}→ARC^{Vglut2} CRACM. Top, schematic of the connection tested. ARC^{AgRP} and ARC^{Vglut2} neurons were transduced with a Cre-dependent ChR2 tagged with mCherry (AAV-DIO-ChR2-mCherry). ChR2-expressing ARC^{AgRP} neurons were identified by co-expression of mCherry and hrGFP (note that NPY expression in the ARC marks all AgRP neurons[47]). ARC^{Vglut2} neurons were identified by expression of mCherry and absence of hrGFP. Bottom, representative traces of light-evoked IPSCs before and after bath application of bicuculline ($GABA_A$ receptor antagonist). $V_h = 0$ mV was used to prevent movement of Na^+ and Ca^{2+} through ChR2 which was expressed in the patched ARC^{Vglut2} neurons, in addition to the afferent ARC^{AgRP} neurons.

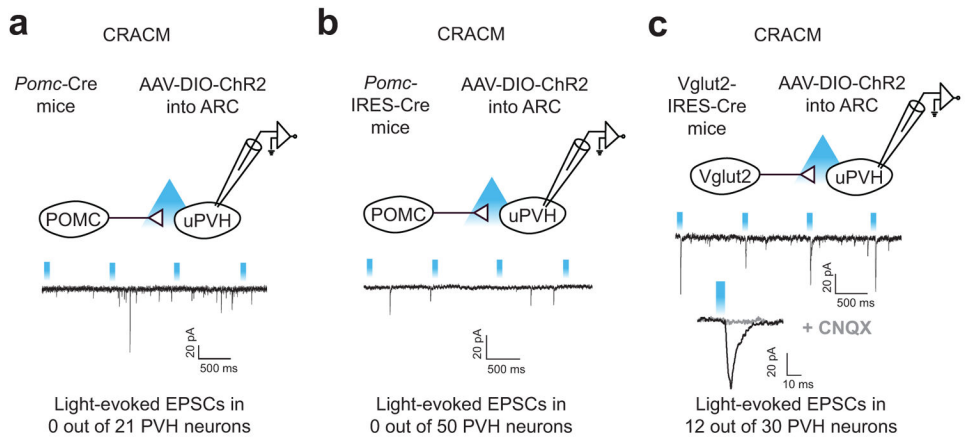

Figure 3. ARC^{Vglut2}→PVH projections, unlike ARC^{POMC}→PVH projections, are effective in glutamatergic transmission

a–c, ARC→PVH CRACM. Top, schematics showing connection being tested. ARC^{POMC} or ARC^{Vglut2} neurons were transduced with Cre-dependent ChR2. Below, representative traces showing assessment of light-evoked EPSCs. **c**, Bottom, representative traces of light-evoked EPSCs before and after bath application of CNQX (AMPAR antagonist)

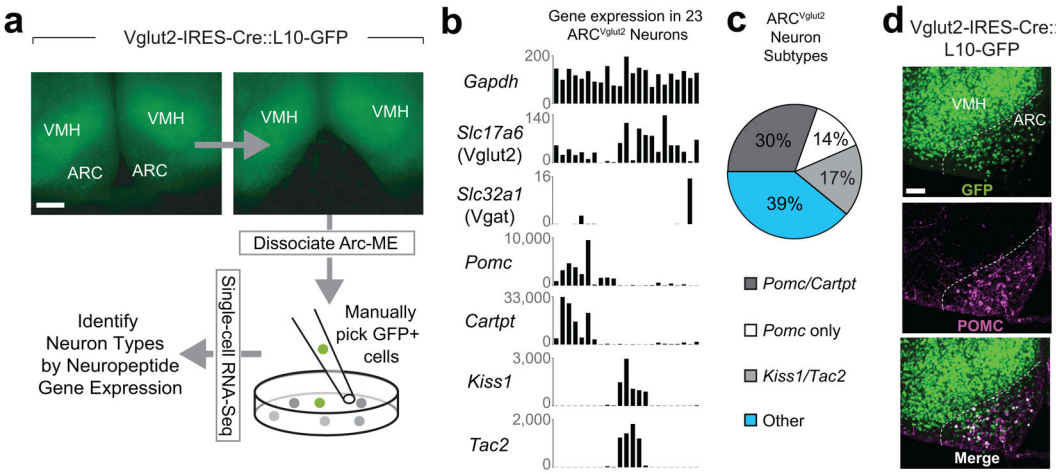

Figure 4. RNA-seq analysis of ARC^{Vglut2} neurons

a, Schematic and representative ARC dissection images for single-cell RNA-seq of GFP-positive ARC^{Vglut2} neurons. Scale bar represents 200 μm and applies to all images. **b**, Detection of housekeeping (*Gapdh*), glutamatergic (*Slc17a6*; Vglut2), GABAergic (*Slc32a1*; Vgat), and selected neuropeptide (*Pomc*, *Cartpt*, *Kiss1*, and *Tac2*) transcripts in ARC^{Vglut2} neurons. Expression values are in units of RPKM (reads per kilobase gene model per million mapped reads). **c**, Percentages of ARC^{Vglut2} neurons that are *Pomc*/*Cartpt, Pomc* only, *Kiss1/Tac2* or "Other" neurons. **d**, Co-localization of POMC and GFP immunoreactivity in the ARC from a Vglut2-IRES-Cre::L10-GFP mouse. Scale bar represents 100 μm and applies to all images.

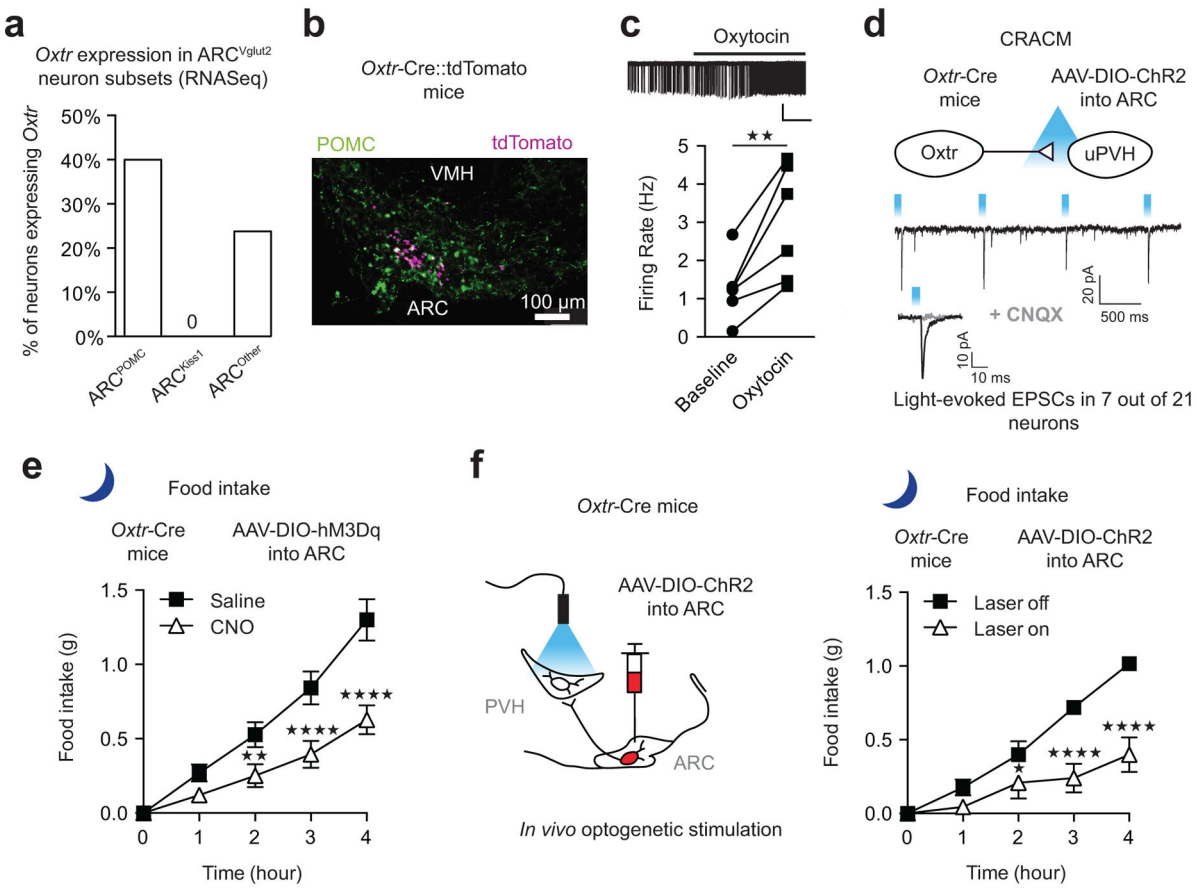

Figure 5. *Oxtr* expression marks ARC$^{\text{Glutamatergic}}$ neurons that rapidly promote satiety

a, *Oxtr* expression in ARC$^{\text{Vglut2}}$ neurons as determined by RNA-seq. **b**, Co-localization of POMC protein in tdTomato-positive ARC$^{\text{Oxtr}}$ neurons. Approximately 50% of ARC$^{\text{Oxtr}}$ neurons expressed POMC. **c**, Representative trace (top) and summary (bottom) of oxytocin's effect on ARC$^{\text{Oxtr}}$ neuron firing rate. Scale bars, 50 pA, 30 sec. 6 slices from 3 mice; mice from multiple litters; cells, $n = 6$. Baseline (M = 1.261, s.d. = 0.8192) versus Oxytocin (M = 2.991, s.d. = 1.495): Paired two-tailed t-test, t(5) = 4.253, $^{**}P = 0.0081$. **d**, CRACM of ARC$^{\text{Oxtr}}$→PVH connectivity. Below, representative traces showing light-evoked EPSCs. **e**, Effect of CNO/hM3Dq stimulation of ARC$^{\text{Oxtr}}$ neurons on dark-cycle feeding ($n = 6$ animals). **f**, Left, experimental schematic. Right, effect of ARC$^{\text{Oxtr}}$ terminal photostimulation in the PVH on dark-cycle feeding ($n = 5$ animals). **e**, **f**, Data are presented as mean ± SEM. Repeated measures two-way ANOVA followed by Sidak's multiple comparisons test. **e**, Mice from multiple litters, $n = 6$ animals. Treatment F(1,5) = 26.25, $P = 0.0037$; time F(4,20) = 63.88, $P < 0.0001$; interaction F(4, 20) = 15.31, $P < 0.0001$.1h, $P = 0.1760$; 2h, $^{**}P = 0.0025$; 3h, $^{****}P < 0.0001$; 4h, $^{****}P < 0.0001$. **f**, Mice from multiple litters, $n = 4$ animals. Repeated measures two-way ANOVA: Treatment F(1,3) = 36.87, $P = 0.0090$; time F(4,12) = 24.90, $P < 0.0001$; interaction F(4, 12) = 14.04, $P = 0.0002$. Sidaks multiple comparisons test: 1h, $P = 0.1276$; 2h, $^{*}P = 0.0195$; 3h, $^{***}P = 0.0001$; 4h, $^{****}P < 0.0001$.

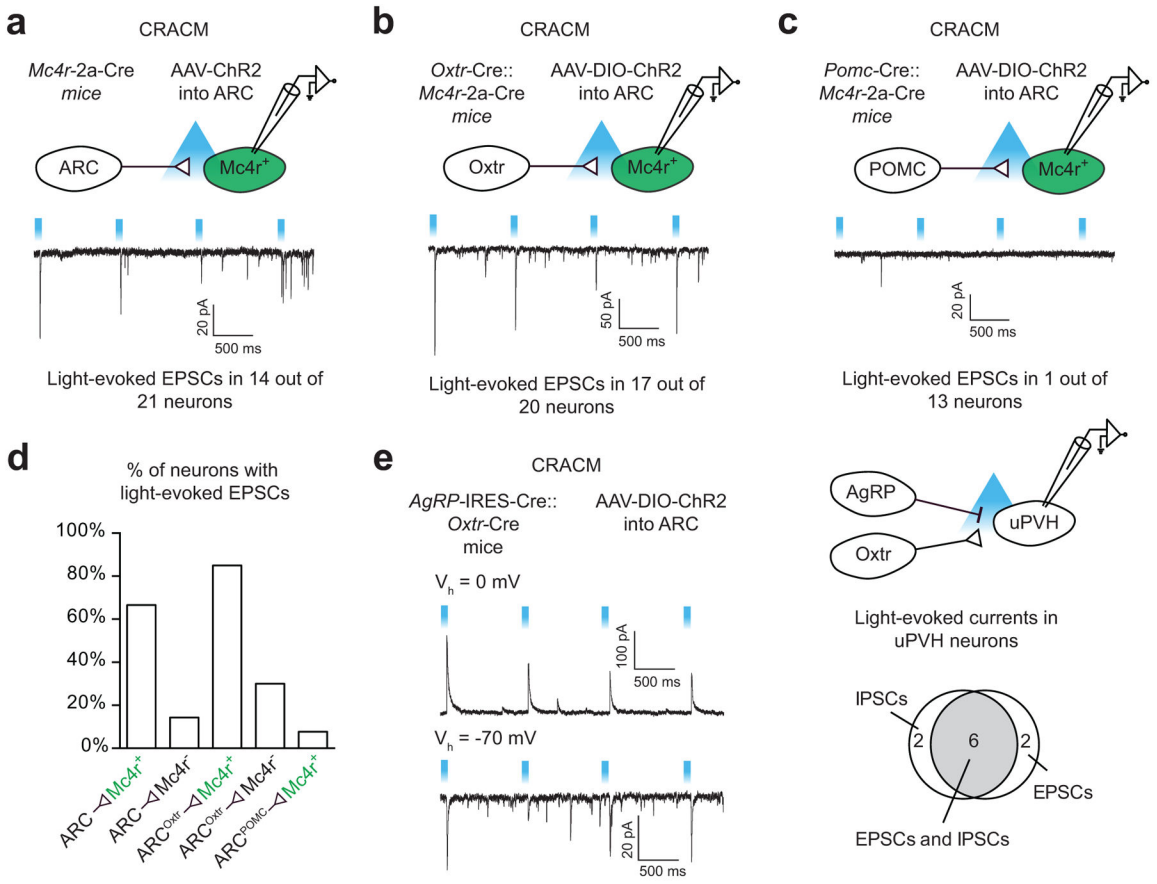

Figure 6. ARC$^{\text{Glutamatergic}}$ and ARC$^{\text{Oxtr}}$ neurons preferentially engage PVH$^{\text{MC4R}}$ neurons

a–c, CRACM of ARC→PVH connectivity. Top, schematics show connections being tested. Below, representative traces showing assessment of light-evoked EPSCs. **d**, Percentage of PVH$^{\text{MC4R+}}$ (MC4R-positive) or PVH$^{\text{MC4R−}}$ (MC4R-negative) neurons with light-evoked EPSCs. **e**, Convergent CRACM of ARC$^{\text{AgRP}}$ and ARC$^{\text{Oxtr}}$ afferents onto PVH neurons. Schematic shown on the top right. Left, representative traces of light-evoked ARC$^{\text{AgRP}}$-mediated IPSCs (top)/ARC$^{\text{Oxtr}}$-mediated EPSCs (bottom) recorded from the same uPVH neuron. Right, Venn diagram summary for all 10 neurons receiving input.

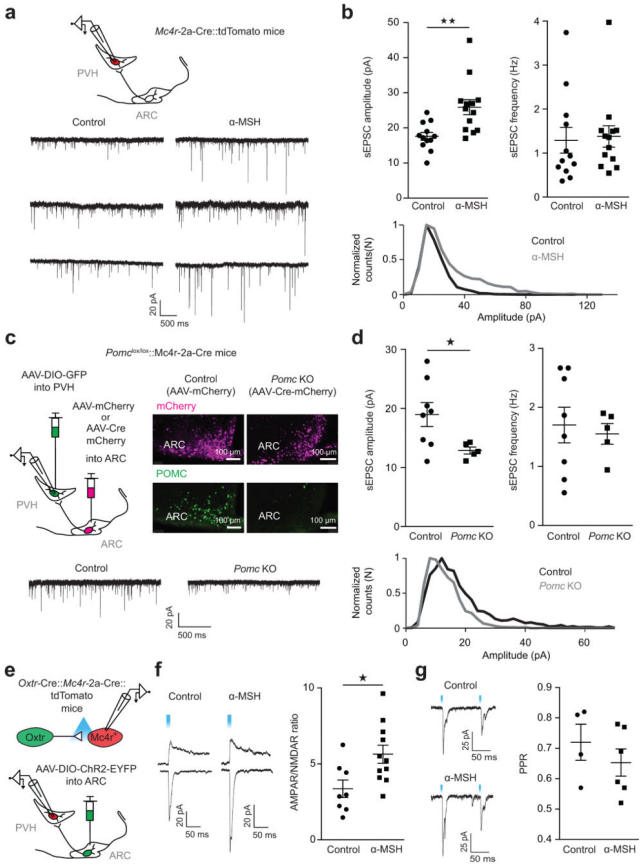

Figure 7. α-MSH post-synaptically increases excitatory input onto PVH^{MC4R} neurons

a, Top, experimental schematic. **a**, **b**, Representative traces (**a,** bottom) and summary (**b**) of α-MSH effects on sEPSCs. 8 slices from 4 mice; mice from multiple litters; sample size (cells): control/α-MSH, n = 12/13. sEPSC amplitude: Control (M = 17.6, s.d. = 3.923) versus α-MSH (M = 25.88, s.d. = 7.668): Unpaired two-tailed t-test, t(23) = 3.353, $^{**}P$ = 0.0028. sEPSC frequency: Control (M = 1.29, s.d. = 1.011) versus α-MSH (M = 1.379, s.d. = 0.8736): Two-tailed Mann-Whitney test: U = 65, P = 0.4951 **b**, Bottom, sEPSC amplitude distribution showing that α-MSH significantly increased the frequency of large-amplitude sEPSCs (Kolmogorov-Smirnov test, P < 0.0001). **c**, Left, experimental schematic. Right, POMC and mCherry immunolabeling in control and *Pomc* knockout (*Pomc* KO) mice. **c**, **d**, Representative traces (**c**, Bottom) and summary (**d**) of *Pomc* KO effects on sEPSCs. Number of slices: Control/Pomc KO, N = 4/4. Number of animals: Control/Pomc KO, N = 2/2. Sample size (cells): Control/Pomc KO, n = 8/5; sEPSC amplitude: Control (M = 18.96, s.d. = 5.721) versus Pomc KO (M = 12.88, s.d. = 1.293): Unpaired two-tailed t-test, t(11)= 2.304, $^{*}P$ = 0.0417. sEPSC frequency: Control (M = 1.703, s.d. = 0.853) versus Pomc KO (M = 1.553, s.d. 0.3897): Unpaired two-tailed t-test: t(11) = 0.3653, P = 0.7218. Bottom, sEPSC distribution showing decreased frequency of large-amplitude sEPSCs in *Pomc* KO mice (Kolmogorov-Smirnov test, P < 0.0001). **e**, Experimental schematic. **f**, **g**, Representative traces (left) and summary (right) of α-MSH effects on light-evoked AMPAR/NMDAR ratios (**f**, slices from 3 mice; mice from multiple litters. Sample size (cells): Control/α-MSH, n = 8/11; Control (M = 3.365, s.d. = 1.622) versus α-MSH (M = 5.642, s.d.

= 1.980): Unpaired two-tailed t-test: t(17) = 2.661, *P = 0.0165) and on light-evoked Paired-Pulse ratios (PPRs) (**g**, Slices from 3 mice; mice from multiple litters. Sample size (cells): control/α-MSH, n = 4/6. Control (M = 0.72, s.d. = 0.1186) versus α-MSH (M = 0.6533, s.d. = 0.1093): Unpaired two-tailed t-test: t(8) = 0.9150, P = 0.387).